



## Flow around a squirmer in a shear-thinning fluid

Kyle Pietrzyk<sup>a</sup>, Herve Nganguia<sup>b</sup>, Charu Datt<sup>d</sup>, Lailai Zhu<sup>c</sup>, Gwynn J. Elfring<sup>d</sup>, On Shun Pak<sup>a,\*</sup>

<sup>a</sup> Department of Mechanical Engineering, Santa Clara University, Santa Clara, CA 95053, USA

<sup>b</sup> Department of Mathematical and Computer Sciences, Indiana University of Pennsylvania, Indiana, PA 15705, USA

<sup>c</sup> KTH Mechanics, Stockholm SE-10044, Sweden

<sup>d</sup> Department of Mechanical Engineering, University of British Columbia, Vancouver, BC V6T 1Z4, Canada

### ARTICLE INFO

**Keywords:**  
Locomotion  
Shear-thinning  
Carreau model

### ABSTRACT

Many biological fluids display shear-thinning rheology, where the viscosity decreases with an increasing shear rate. To better understand how this non-Newtonian rheology affects the motion of biological and artificial microswimmers, recent efforts have begun to seek answers to fundamental questions about active bodies in shear-thinning fluids. Previous analyses based on a squirmer model have revealed non-trivial variations of propulsion characteristics in a shear-thinning fluid via the reciprocal theorem. However, the reciprocal theorem approach does not provide knowledge about the flow surrounding the squirmer. In this work, we fill in this missing information by calculating the non-Newtonian correction to the flow analytically in the asymptotic limit of small Carreau number. In particular, we investigate the local effect due to viscosity reduction and the non-local effect due to induced changes in the flow; we then quantify their relative importance to locomotion in a shear-thinning fluid. Our results demonstrate cases where the non-local effect can be more significant than the local effect. These findings suggest that caution should be exercised when developing physical intuition from the local viscosity distribution alone around a swimmer in a shear-thinning fluid.

### 1. Introduction

Locomotion of microorganisms is subject to often unintuitive constraints imposed by physics at the scales of the microscopic world [1]. Inertial effects, which govern macroscopic locomotion, become subdominant to viscous forces at small scales. Reynolds numbers, which characterize the inertial to viscous force, typically range between  $10^{-6}$  for flagellated bacteria to  $10^{-2}$  for spermatozoa [2]. Microorganisms have evolved strategies to move through fluids for diverse biological processes such as reproduction and foraging [3]. Extensive theoretical and experimental studies have sought to elucidate physical principles that underlie cell motility [4–6]. This has improved our general understanding of low-Reynolds-number locomotion, which in recent years has led to the development of a variety of synthetic micro-propellers. While some micro-propellers are bio-mimetic or bio-inspired, others exploit physical and physico-chemical mechanisms to achieve micro-propulsion [7–12]. Considerable progress over the last several decades has illuminated low-Reynolds-number locomotion in Newtonian fluids [5,13]. However, biological fluids often display complex (non-Newtonian) rheological properties that include viscoelasticity and shear-thinning viscosity [14–16]. A fundamental understanding of how non-Newtonian fluid rheology affects propulsion is imperative to both deciphering the

roles of mechanical forces in cell motility and designing synthetic microswimmers for realistic biological media [17,18].

Over the past decade, studies on locomotion in complex fluids have largely focused on the effect of viscoelastic stresses [19–27]. Much less is known about locomotion in shear-thinning fluids [18]. Many biological fluids, including blood and mucus, are shear thinning: the fluid becomes less viscous with applied strain rates due to changes in the fluid microstructure [28]. Previous theoretical and experimental studies on undulatory swimmers (e.g. sheets [29–33], filaments [34], and nematodes [35–37]), helical propellers [38], squirmers [31,39–41], single-hinged swimmers [42], and a variety of two-dimensional swimmers [30,31] have revealed that shear-thinning rheology can enhance or hinder locomotion depending on the class of swimmer and its swimming gait. More recently, Montenegro-Johnson [43] emphasized that generalizing insights gained from two-dimensional modeling in shear-thinning fluids to the three-dimensional case should be handled with care, because the flow derivatives in these two cases can be drastically different. Numerical studies have also begun to address locomotion in shear-thinning fluids in the presence of a confining boundary [44] and inertial effects [45].

In our previous studies [39,41], we considered the locomotion of a spherical body propelling itself with surface distortions (known as a

\* Corresponding author.

E-mail addresses: [gelfring@mech.ubc.ca](mailto:gelfring@mech.ubc.ca) (G.J. Elfring), [opak@scu.edu](mailto:opak@scu.edu) (O.S. Pak).

squirmers) in a shear-thinning fluid via the reciprocal theorem [46–49]. Despite the success of the reciprocal theorem approach in revealing non-trivial variations of propulsion characteristics in a shear-thinning fluid, this approach does not yield information about the flow around the squirmer. This prevents subsequent analyses on the effects of flow advection on nutrient uptake by microorganisms or phoretic motion of active particles in a shear-thinning fluid. In this paper, we fill in this missing information by deriving a closed-form, analytical solution to the flow around a squirmer in a shear-thinning fluid in a weakly non-Newtonian regime. The knowledge of the surrounding flow allows more detailed analyses of the physical changes when the fluid becomes shear-thinning. The shear-thinning effect can manifest through two types of physical changes: the first change is the local effect of stress modulation due to viscosity differences, and the second change is the non-local effect resulting from overall changes to the fluid flow [34,38]. A recent empirical resistive-force theory for slender filaments in shear-thinning fluids has focused on the first of these two effects and obtained qualitative agreements with experimental results [34]. The asymptotic analysis here allows us to decouple the local and non-local effects, in the weakly non-Newtonian limit, and hence quantify their relative importance to locomotion in a shear-thinning fluid via a squirmer model. The changes in the flow fields are also likely to impact hydrodynamic interactions with nearby swimmers but we leave it to future work to examine rheological effects on collective locomotion.

The paper is organized as follows. In Section 2, we formulate the problem by introducing the squirmer model (Section 2.1), the rheological constitutive model (Section 2.2), and the asymptotic analysis (Section 2.3) considered in this work. In Section 3, we present results on the flow around a two-mode squirmer in a shear-thinning fluid. Next, we discuss in Section 4 how shear-thinning rheology can enable other squirming modes to contribute to propulsion, followed by a detailed analysis of the flow around a squirmer. Concluding remarks are presented in Section 5.

## 2. Formulation

### 2.1. Squirmer model

Lighthill [50] and Blake [51] first modeled ciliary propulsion by the motion of a squirming sphere, which is arguably the simplest possible three-dimensional swimmer of finite size. The motion of beating cilia is represented as a distribution of velocities on the squirmer surface. For a steady spherical squirmer of radius  $a$ , the tangential, time-independent surface velocity distribution is decomposed into a series of the form [52]

$$u_\theta(r = a, \theta) = \sum_{k=1}^{\infty} -\frac{2}{k(k+1)} B_k P_k^1(\cos \theta), \quad (1)$$

where  $P_k^1$  represents the associated Legendre function of the first kind,  $\theta$  is the polar angle measured from the axis of symmetry, and the squirming modes  $B_k$  are related to singularity solutions in Stokes flows. In a Newtonian fluid, only the  $B_1$  mode (a source dipole) contributes to the propulsion speed  $U_N = 2B_1/3$ , and the  $B_2$  mode (a force dipole) is the slowest decaying spatial mode that dominates the far-field velocity generated by a squirmer. Therefore, many studies considered model swimmers represented by only the first two modes of the expansion [52].

Although the squirmer model was developed originally for swimming ciliates (such as *Volvox* [53]), it has also gained popularity as a general model for active particles [54–60]. The parameters in the squirming modes can be adjusted to represent different types of swimmers, broadly categorized as pushers ( $\alpha = B_2/B_1 < 0$ ), pullers ( $\alpha > 0$ ), and neutral squirmers ( $\alpha = 0$ ). A pusher, such as the bacterium *Escherichia coli*, obtains its thrust from the rear part of the body. A puller, such as the alga *Chlamydomonas*, obtains its thrust from the front part. A neutral squirmer generates a surrounding flow corresponding to a source dipole. While we prescribe the surface velocity of the swimmer here, the gait of

a real microorganism is likely to be modified by changes in stresses due to shear thinning.

### 2.2. Governing equations

The incompressible flow around a squirmer in a shear-thinning fluid at low Reynolds numbers is governed by the continuity equation and Cauchy's equation of motion

$$\nabla \cdot \mathbf{u} = 0, \quad (2)$$

$$\nabla \cdot \boldsymbol{\sigma} = \mathbf{0}, \quad (3)$$

where the stress tensor,  $\boldsymbol{\sigma} = -p\mathbf{I} + \boldsymbol{\tau}$ . Rheological data of some biological fluids has been shown to be consistent with the Carreau model [28,32,61]:

$$\boldsymbol{\tau} = \eta_0 \dot{\boldsymbol{\gamma}} - (\eta_0 - \eta_\infty) \left[ 1 - (1 + \lambda_t^2 |\dot{\boldsymbol{\gamma}}|^2)^{\frac{n-1}{2}} \right] \dot{\boldsymbol{\gamma}}. \quad (4)$$

Here,  $\eta_0$  and  $\eta_\infty$  represent the zero and infinite-shear rate viscosities, respectively, and  $\dot{\boldsymbol{\gamma}}$  denotes the strain rate tensor. The magnitude of the strain rate tensor is given by  $|\dot{\boldsymbol{\gamma}}| = (\dot{\gamma}_{ij}\dot{\gamma}_{ij}/2)^{1/2}$ . The power law index  $n < 1$  characterizes the degree of shear-thinning, and the time constant  $\lambda_t$  sets the crossover strain rate at which the non-Newtonian behavior becomes significant. For example, (shear-) rheological measurements of human cervical mucus can be fit to the Carreau model with values  $\eta_0 = 145.7$  Pa s,  $\eta_\infty = 0$  Pa s,  $\lambda_t = 631.04$  s and  $n = 0.27$  [32,61].

For a prescribed velocity distribution on the squirmer surface ( $r = a$ ) given by Eq. (1), the squirmer propels with an unknown velocity  $\mathbf{U} = U\mathbf{e}_z$  along its axis of symmetry. In a reference frame moving with the squirmer (i.e., the co-moving frame), the far-field condition is given by the unknown propulsion velocity  $\mathbf{u}(r \rightarrow \infty) = -\mathbf{U}$ . The mathematical formulation is completed by enforcing the force-free

$$\int_S \boldsymbol{\sigma} \cdot \mathbf{n} \, dS = \mathbf{0}, \quad (5)$$

and torque-free conditions for self-propulsion at low Reynolds numbers, where  $\mathbf{n}$  represents the unit normal vector on the squirmer surface  $S$ . The torque-free condition is satisfied automatically as a result of the axisymmetry in this problem.

In general, the motion of a force-free, axisymmetric swimmer in a non-Newtonian fluid with a constitutive equation of the form  $\boldsymbol{\tau} = \eta_0 \dot{\boldsymbol{\gamma}} + \boldsymbol{\tau}^{\text{NN}}$ , where  $\boldsymbol{\tau}^{\text{NN}}$  denotes the additional non-Newtonian stress (e.g., Eq. (4)), satisfies

$$\mathbf{U} = \mathbf{R}^{-1} \cdot [\mathbf{F}^{\text{T}} + \mathbf{F}^{\text{NN}}]. \quad (6)$$

Here  $\mathbf{R} = 6\pi\eta_0 a \mathbf{I}$  is the translational resistance of a sphere in a Newtonian fluid with viscosity  $\eta_0$ ;  $\mathbf{F}^{\text{T}}$  represents the propulsive thrust the swimmer would generate in a Newtonian fluid (with viscosity  $\eta_0$ );  $\mathbf{F}^{\text{NN}}$  is the non-Newtonian force that results from changes in viscosity from  $\eta_0$  (due to  $\boldsymbol{\tau}^{\text{NN}}$ , the second term on the right-hand side of Eq. (4)). As discussed in Section 1, the non-Newtonian force may be split into local and non-local contributions  $\mathbf{F}^{\text{NN}} = \mathbf{F}^{\text{L}} + \mathbf{F}^{\text{NL}}$ . The first weakly non-linear correction to the Newtonian swimming speed can be determined readily without solving the complex fluid flow by the reciprocal theorem [39,62], but in what follows we solve for corrections to the flow field itself, due to small changes in viscosity from  $\eta_0$ , in order to develop better physical intuition on the nature of the local and non-local non-Newtonian forces.

### 2.3. Asymptotic analysis

We non-dimensionalize lengths by the squirmer radius  $a$ , velocities by the first mode of actuation  $B_1$  except when the surface actuation does not contain a  $B_1$  mode (e.g., in Section 4, where only the third mode of actuation,  $B_3$ , is considered), strain rates by  $\omega = B_1/a$  and stresses by  $\eta_0\omega$ . The dimensionless constitutive equation then takes the form

$$\boldsymbol{\tau}^* = \dot{\boldsymbol{\gamma}}^* - (1 - \beta) \left[ 1 - (1 + Cu^2 |\dot{\boldsymbol{\gamma}}^*|^2)^{\frac{n-1}{2}} \right] \dot{\boldsymbol{\gamma}}^*, \quad (7)$$

where the viscosity ratio  $\beta = \eta_\infty/\eta_0$ . The Carreau number,  $Cu = \lambda_c\omega$ , compares the characteristic strain rate  $\omega$  to the crossover strain rate  $1/\lambda_c$ . Hereafter, we drop the stars for simplicity and refer to only dimensionless variables unless otherwise stated.

To make analytical progress, we conduct an asymptotic analysis for small Carreau numbers ( $Cu^2 \ll 1$ ) and expand the swimming speed and all fields in regular perturbation series in powers of  $Cu^2$ :

$$\{\mathbf{u}, p, \dot{\gamma}, \boldsymbol{\tau}, \boldsymbol{\sigma}, \mathbf{U}\} = \{\mathbf{u}_0, p_0, \dot{\gamma}_0, \boldsymbol{\tau}_0, \boldsymbol{\sigma}_0, \mathbf{U}_0\} + Cu^2\{\mathbf{u}_1, p_1, \dot{\gamma}_1, \boldsymbol{\tau}_1, \boldsymbol{\sigma}_1, \mathbf{U}_1\} + O(Cu^4). \tag{8}$$

By substituting these expansions into the governing equations and boundary conditions, we solve the non-Newtonian problem perturbatively to obtain the detailed flow surrounding the squirmer order by order.

### 3. Flow around a two-mode squirmer at small $Cu$

In this section, we consider the squirming motion of a two-mode squirmer ( $\alpha = B_2/B_1$ ) in a shear-thinning fluid in the small  $Cu$  limit.

#### 3.1. Zeroth-order solution

The  $O(Cu^0)$  solution is governed by the Stokes equations

$$\nabla \cdot \mathbf{u}_0 = 0, \tag{9}$$

$$\nabla \cdot \boldsymbol{\sigma}_0 = \mathbf{0}, \tag{10}$$

where  $\boldsymbol{\sigma}_0 = -p_0\mathbf{I} + \dot{\gamma}_0$ , with the far-field and boundary conditions on the squirmer given by

$$\mathbf{u}_0(r=1) = u_\theta e_\theta, \quad \mathbf{u}_0(r \rightarrow \infty) = -\mathbf{U}_0. \tag{11}$$

Here we consider the first two modes ( $B_1$  and  $B_2$ ) of the surface velocity  $u_\theta$  in Eq. (1). The dimensionless surface velocity (scaled by  $B_1$ ) of a two-mode squirmer is given by  $u_\theta(r=1) = \sin\theta + \alpha(\sin 2\theta)/2$ .

The solution to this problem,  $\mathbf{u}_0 = u_0 e_r + v_0 e_\theta$ , was obtained by Lighthill [50] and Blake [51] as

$$u_0 = U_0 \left( \frac{1}{r^3} - 1 \right) \cos\theta + \frac{\alpha}{2} \left( \frac{1}{r^4} - \frac{1}{r^2} \right) (3 \cos^2\theta - 1), \tag{12}$$

$$v_0 = U_0 \left( 1 + \frac{1}{2r^3} \right) \sin\theta + \frac{\alpha}{r^4} \cos\theta \sin\theta, \tag{13}$$

with the pressure field given by

$$p_0 = -\frac{\alpha[1 + 3 \cos 2\theta]}{2r^3}. \tag{14}$$

By enforcing the force-free condition  $\int_S \boldsymbol{\sigma}_0 \cdot \mathbf{n} \, dS = \mathbf{0}$ , the unknown swimming speed (scaled by  $B_1$ ) is given by  $U_0 = 2/3$ . We highlight again that, among all squirming modes, only the  $B_1$  mode contributes to self-propulsion in Stokes flow.

#### 3.2. First-order solution

The  $O(Cu^2)$  solution is governed by the equations

$$\nabla \cdot \mathbf{u}_1 = 0, \tag{15}$$

$$\nabla \cdot \boldsymbol{\sigma}_1 = \mathbf{0}, \tag{16}$$

where  $\boldsymbol{\sigma}_1 = -p_1\mathbf{I} + \dot{\gamma}_1 + \mathbf{A}$  and

$$\mathbf{A} = \frac{(1-\beta)(n-1)}{2} |\dot{\gamma}_0|^2 \dot{\gamma}_0. \tag{17}$$

The solution is subject to the far-field and boundary conditions

$$\mathbf{u}_1(r=1) = \mathbf{0}, \quad \mathbf{u}_1(r \rightarrow \infty) = -\mathbf{U}_1. \tag{18}$$

Here, we note that the surface velocity distribution has been already accounted for in the  $O(Cu^0)$  calculations, leaving no-slip and no-penetration boundary conditions on the squirmer surface at this order.

We note that, under this asymptotic expansion, the changes in the flow fields are linear in the parameters  $n$  and  $\beta$  at first order.

We take the curl of (16) to eliminate pressure and obtain the equation

$$\nabla \times (\nabla \cdot \dot{\gamma}_1) = -\frac{(1-\beta)(n-1)}{2} \{ \nabla \times [\nabla \cdot (|\dot{\gamma}_0|^2 \dot{\gamma}_0)] \}. \tag{19}$$

Due to the axisymmetry of the problem, we can express the velocity field  $\mathbf{u} = u_1 e_r + v_1 e_\theta$  in terms of Stokes streamfunction

$$u_1 = \frac{1}{r^2 \sin\theta} \frac{\partial \psi_1}{\partial \theta}, \quad v_1 = -\frac{1}{r \sin\theta} \frac{\partial \psi_1}{\partial r}, \tag{20}$$

to satisfy the continuity equation, Eq. (15). The momentum equation in terms of Stokes streamfunction therefore becomes

$$E^2(E^2 \psi_1) = \frac{(1-\beta)(n-1)}{2} r \sin\theta \{ \nabla \times [\nabla \cdot (|\dot{\gamma}_0|^2 \dot{\gamma}_0)] \}, \tag{21}$$

where the operator

$$E^2 \equiv \frac{\partial^2}{\partial r^2} + \frac{\sin\theta}{r^2} \frac{\partial}{\partial \theta} \left( \frac{1}{\sin\theta} \frac{\partial}{\partial \theta} \right). \tag{22}$$

We assume a solution of the form

$$\psi_1 = (1-\beta)(n-1) \sin^2\theta \sum_{i=0}^{\infty} f_i(r) T_i(\cos\theta), \tag{23}$$

where  $f_i(r)$  are unknown functions of  $r$  and  $T_i(\cos\theta)$  are Chebyshev polynomials. By substituting this assumed solution into Eq. (21) we obtain a system of ordinary differential equations for  $f_i(r)$ . We solve this system of equations and determine the unknown coefficients by the far-field and boundary conditions, Eq. (18) (see Appendix A for details).

The streamfunction for the flow around a squirmer with just the  $B_1$  mode ( $\alpha = 0$ ) is given by

$$\begin{aligned} \psi_1 = & -(1-\beta)(n-1) \sin^2\theta \left[ \frac{c_1^{B_1}}{r^9} + \frac{c_2^{B_1}}{r^3} + \frac{c_3^{B_1}}{r} + c_4^{B_1} r \right. \\ & \left. + \cos 2\theta \left( \frac{c_5^{B_1}}{r^9} + \frac{c_6^{B_1}}{r^3} + \frac{c_7^{B_1}}{r} \right) \right] \\ & - \frac{\sin^2\theta}{4} \left( \frac{1}{r} - 3r + 2r^2 \right) U_1, \end{aligned} \tag{24}$$

while the pressure field is given by

$$\begin{aligned} p_1 = & \frac{(1-\beta)(n-1)}{2} \left[ \frac{e_1^{B_1}}{r^{12}} + \frac{e_2^{B_1}}{r^4} + \frac{e_3^{B_1}}{r^2} + \cos 2\theta \left( \frac{e_4^{B_1}}{r^{12}} + \frac{e_5^{B_1}}{r^4} \right) \right] \cos\theta \\ & + \frac{3}{2r^2} U_1 \cos\theta. \end{aligned} \tag{25}$$

The coefficients  $c_i^{B_1}$  and  $e_i^{B_1}$  are tabulated in Table C.1. The expressions for the streamfunction and the pressure of the flow around a squirmer with both  $B_1$  and  $B_2$  modes are far lengthier and therefore are given in Appendix B.

By applying the force-free condition  $\int_S \boldsymbol{\sigma}_1 \cdot \mathbf{n} \, dS = \mathbf{0}$ , we determine the first non-Newtonian correction to the propulsion speed of a two-mode squirmer as

$$U_1 = (1-\beta)(n-1) \frac{4(616 + 1383\alpha^2)}{15015}, \tag{26}$$

which agrees with the result in [39] using the reciprocal theorem thereby providing a consistency check on the flow field calculations. Fig. 1 displays the zeroth-order flow field (Newtonian) and its first non-Newtonian correction around a neutral squirmer (a & b) and a two-mode squirmer (c & d).

### 4. Flow around a third-mode squirmer at small $Cu$

In this section, we consider surface velocity distributions other than the first two modes. In Stokes flow, only the  $B_1$  mode leads to net motion

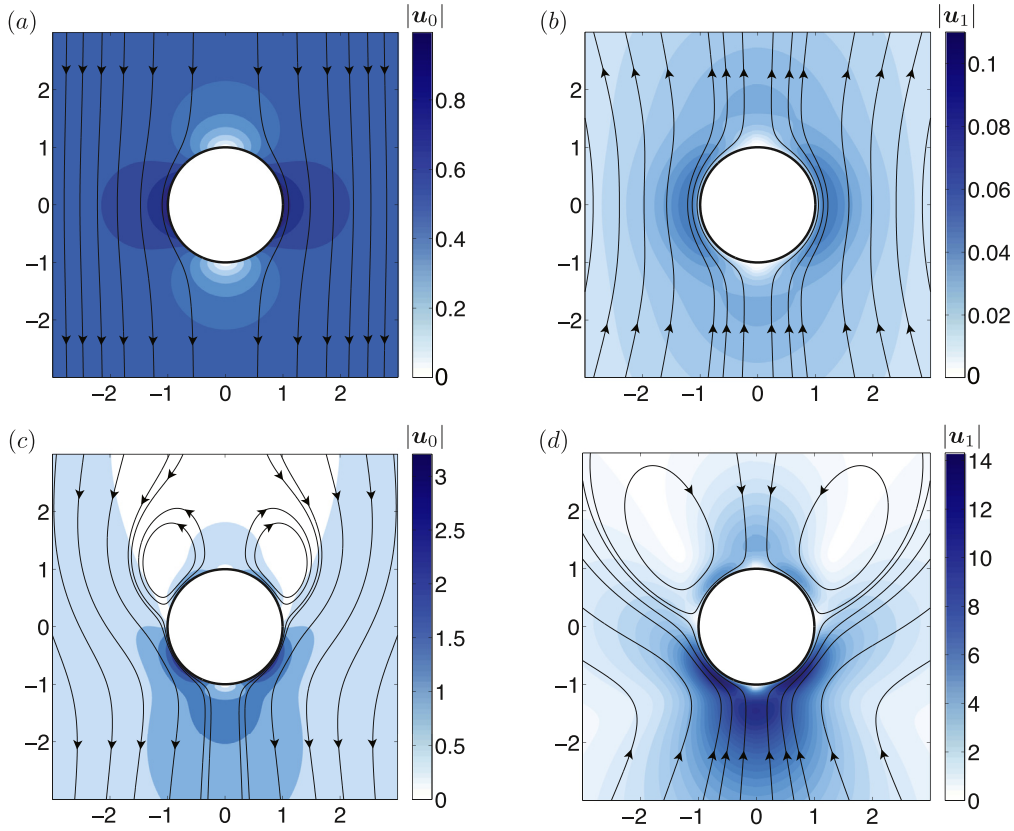


**Fig. 1.** Streamlines and local speed of the flow around a neutral squirmer (a & b) and a pusher (c & d) in the co-moving frame. For the neutral squirmer ( $\alpha = B_2/B_1 = 0$ ): (a) zeroth-order velocity field (Stokes flow), and (b) first-order velocity field. For the pusher ( $\alpha = -5$ ): (c) zeroth-order velocity field (Stokes flow), and (d) first-order velocity field. Both squirmers propel with positive zeroth-order velocities ( $U_0 > 0$ , upward) in (a) and (c) and negative first-order corrections ( $U_1 < 0$ ) in (b) and (d). Here  $n = 0.25$ ,  $\beta = 0.5$ . Note that the first-order fields exclude the  $Cu^2$  prefactor.

of a squirmer while the first even mode,  $B_2$ , is often retained to represent the far-field contribution. Higher squirming modes are not typically considered when analyzing squirming swimmers in Newtonian fluids. We note that any even squirming mode alone does not contribute to self-propulsion in Newtonian or shear-thinning fluids due to the symmetry of the surface velocity distribution. The  $B_3$  mode, hence, is the first squirming mode that could lead to self-propulsion in a shear-thinning fluid but not in a Newtonian fluid; in this case, the Newtonian thrust  $F^T = 0$ , and the motion of the squirmer is due to  $F^{NN}$  alone, as shown in Eq. (6). Here we present a detailed analysis of the propulsion and flow around a squirmer with only a  $B_3$  mode, calculate  $F^{NN}$ , and discuss the relative contributions of the local and non-local non-Newtonian forces. We note that velocities in this section are non-dimensionalized by the third mode of actuation  $B_3$ .

#### 4.1. Zeroth-order solution

Using the same set of equations in Stokes flows (Eqs. (9) and (10)), boundary conditions (Eq. (11)), and force-free condition  $\int_S \sigma_0 \cdot n \, dS = 0$ , the  $O(Cu^0)$  flow is calculated as [50,51]

$$u_0 = \frac{1}{2} \left( \frac{1}{r^5} - \frac{1}{r^3} \right) (5 \cos^3 \theta - 3 \cos \theta), \quad (27)$$

$$v_0 = \frac{1}{8} \left( \frac{1}{r^5} - \frac{1}{3r^3} \right) (15 \cos^2 \theta - 3) \sin \theta, \quad (28)$$

with the pressure field given by

$$p_0 = -\frac{1}{8r^4} (5 - 25 \cos 2\theta) \cos \theta. \quad (29)$$

The force-free condition is satisfied with a zero swimming velocity  $U_0 = 0$ , i.e., a third-mode squirmer does not propel in Stokes flows. Fig. 2a & c display the zeroth-order velocity and pressure fields, respectively.

#### 4.2. First-order solution

We follow the same approach outlined in Section 3.2 to determine the streamfunction of the flow around a third-mode squirmer at  $O(Cu^2)$  to be

$$\begin{aligned} \psi_1 = & -(1 - \beta)(n - 1) \sin^2 \theta \left[ \frac{c_1^{B_3}}{r^{15}} + \frac{c_2^{B_3}}{r^{13}} + \frac{c_3^{B_3}}{r^{11}} + \frac{c_4^{B_3}}{r^9} + \frac{c_5^{B_3}}{r^7} + \frac{c_6^{B_3}}{r^5} + \frac{c_7^{B_3}}{r^3} \right. \\ & + \frac{c_8^{B_3}}{r} + c_9^{B_3} r + c_{10}^{B_3} \frac{\log r}{r^9} \\ & + \cos 2\theta \left( \frac{c_{11}^{B_3}}{r^{15}} + \frac{c_{12}^{B_3}}{r^{13}} + \frac{c_{13}^{B_3}}{r^{11}} + \frac{c_{14}^{B_3}}{r^9} + \frac{c_{15}^{B_3}}{r^7} + \frac{c_{16}^{B_3}}{r^5} + \frac{c_{17}^{B_3}}{r^3} + \frac{c_{18}^{B_3}}{r} + c_{19}^{B_3} \frac{\log r}{r^9} \right) \\ & + \cos 4\theta \left( \frac{c_{20}^{B_3}}{r^{15}} + \frac{c_{21}^{B_3}}{r^{13}} + \frac{c_{22}^{B_3}}{r^{11}} + \frac{c_{23}^{B_3}}{r^9} + \frac{c_{24}^{B_3}}{r^7} + \frac{c_{25}^{B_3}}{r^5} + \frac{c_{26}^{B_3}}{r^3} + c_{27}^{B_3} \frac{\log r}{r^9} \right) \\ & + \cos 6\theta \left( \frac{c_{28}^{B_3}}{r^{15}} + \frac{c_{29}^{B_3}}{r^{13}} + \frac{c_{30}^{B_3}}{r^{11}} + \frac{c_{31}^{B_3}}{r^9} + \frac{c_{32}^{B_3}}{r^7} + \frac{c_{33}^{B_3}}{r^5} + c_{34}^{B_3} \frac{\log r}{r^9} \right) \\ & + \cos 8\theta \left( \frac{c_{35}^{B_3}}{r^{15}} + \frac{c_{36}^{B_3}}{r^{13}} + \frac{c_{37}^{B_3}}{r^{11}} + \frac{c_{38}^{B_3}}{r^9} + \frac{c_{39}^{B_3}}{r^7} + c_{40}^{B_3} \frac{\log r}{r^9} \right) \\ & \left. - \frac{\sin^2 \theta}{4} \left( \frac{1}{r} - 3r + 2r^2 \right) U_1. \right] \quad (30) \end{aligned}$$

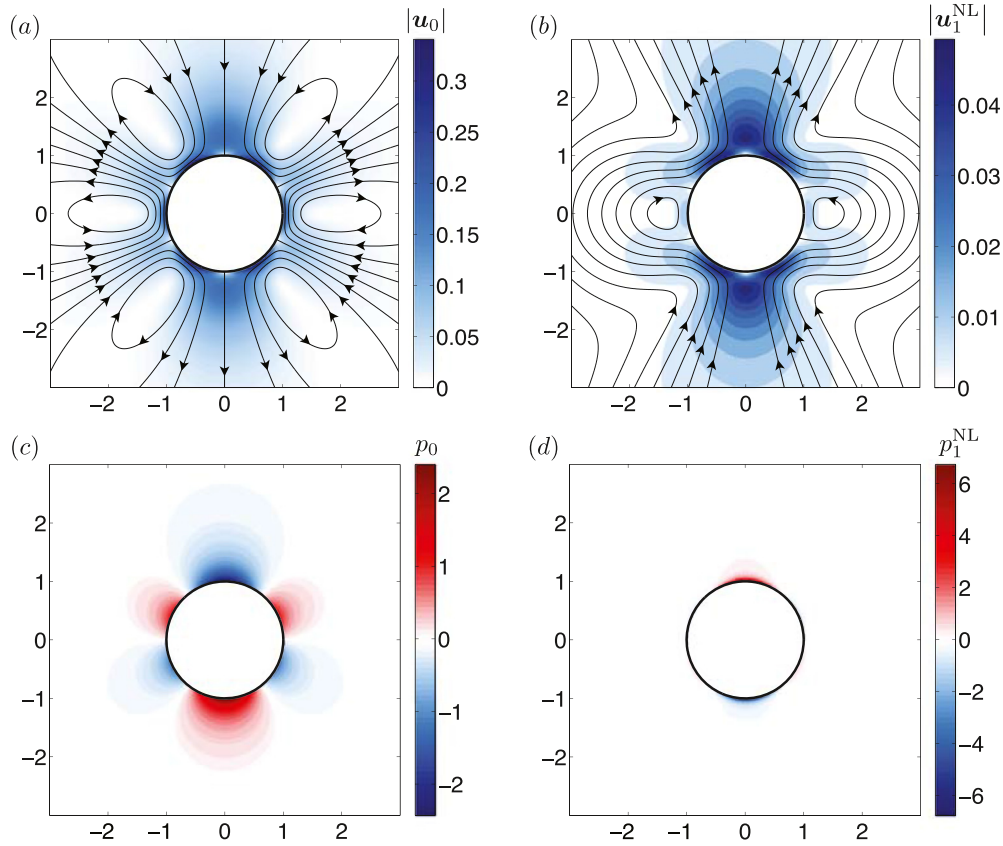


**Fig. 2.** Streamlines and local speed of the flow around a squirmer with a positive  $B_3$  mode in the co-moving frame: (a) zeroth-order velocity field (Stokes flow); (b) non-local first-order velocity field; (c) zeroth-order pressure field (Stokes flow); (d) non-local first-order pressure field. Here  $n = 0.25, \beta = 0.5$ . Shear-thinning rheology enables the third-mode squirmer, which does not generate any net motion in Stokes flow ( $U_0 = 0$ ), to self-propel with a negative first-order velocity ( $U_1 < 0$ , downward) in (b). Note that the first-order fields exclude the  $Cu^2$  prefactor.

The pressure field is given by

$$\begin{aligned}
 p_1 = & \frac{(1-\beta)(n-1)}{2} \cos \theta \left[ \frac{e_1^{B_3}}{r^{18}} + \frac{e_2^{B_3}}{r^{16}} + \frac{e_3^{B_3}}{r^{14}} + \frac{e_4^{B_3}}{r^{12}} + \frac{e_5^{B_3}}{r^{10}} + \frac{e_6^{B_3}}{r^8} + \frac{e_7^{B_3}}{r^6} + \frac{e_8^{B_3}}{r^4} \right. \\
 & \left. + \frac{e_9^{B_3}}{r^2} + \cos 2\theta \left( \frac{e_{10}^{B_3}}{r^{18}} + \frac{e_{11}^{B_3}}{r^{16}} + \frac{e_{12}^{B_3}}{r^{14}} + \frac{e_{13}^{B_3}}{r^{12}} + \frac{e_{14}^{B_3}}{r^{10}} + \frac{e_{15}^{B_3}}{r^8} + \frac{e_{16}^{B_3}}{r^6} + \frac{e_{17}^{B_3}}{r^4} \right) \right. \\
 & \left. + \cos 4\theta \left( \frac{e_{18}^{B_3}}{r^{18}} + \frac{e_{19}^{B_3}}{r^{16}} + \frac{e_{20}^{B_3}}{r^{14}} + \frac{e_{21}^{B_3}}{r^{12}} + \frac{e_{22}^{B_3}}{r^{10}} + \frac{e_{23}^{B_3}}{r^8} + \frac{e_{24}^{B_3}}{r^6} \right) \right. \\
 & \left. + \cos 6\theta \left( \frac{e_{25}^{B_3}}{r^{18}} + \frac{e_{26}^{B_3}}{r^{16}} + \frac{e_{27}^{B_3}}{r^{14}} + \frac{e_{28}^{B_3}}{r^{12}} + \frac{e_{29}^{B_3}}{r^{10}} + \frac{e_{30}^{B_3}}{r^8} \right) \right. \\
 & \left. + \cos 8\theta \left( \frac{e_{31}^{B_3}}{r^{18}} + \frac{e_{32}^{B_3}}{r^{16}} + \frac{e_{33}^{B_3}}{r^{14}} + \frac{e_{34}^{B_3}}{r^{12}} + \frac{e_{35}^{B_3}}{r^{10}} \right) \right] + \frac{3}{2r^2} U_1 \cos \theta. \quad (31)
 \end{aligned}$$

The coefficients  $c_i^{B_3}$  and  $e_i^{B_3}$  are tabulated in Table C.3.

By applying the force-free condition  $\int_S \sigma_1 \cdot n \, dS = \mathbf{0}$ , we determine the swimming speed of a third-mode squirmer at  $O(Cu^2)$ ,

$$U_1 = (1-\beta)(n-1) \frac{1079072}{53348295}, \quad (32)$$

where the speed is made dimensionless by the value of  $B_3$ . For a positive  $B_3$  mode, a squirmer swims in the negative  $z$ -direction in a shear-thinning fluid ( $n < 1$ ). This example demonstrates that shear-thinning rheology can render ineffective swimming gaits in Newtonian fluid (e.g., the  $B_3$  mode) useful in a non-Newtonian fluid. Similar calculations can be performed on other odd squirming modes.

### 4.3. Flow analysis around a squirmer

The shear-thinning effect can manifest through two types of physical changes when a fluid has shear-thinning viscosities: a local effect due to viscosity reduction and a non-local effect due to induced changes in the flow. In this section, we utilize knowledge of the flow around a squirmer to quantify these effects.

We expanded the fluid stress  $\sigma = \sigma_0 + Cu^2 \sigma_1 + O(Cu^4)$  in the small  $Cu$  limit, where the first non-Newtonian correction to stress is given by

$$\sigma_1 = -p_1 \mathbf{I} + \dot{\gamma}_1 + \mathbf{A}. \quad (33)$$

The contribution by  $-p_1 \mathbf{I} + \dot{\gamma}_1$  to  $\sigma_1$  in Eq. (33) depends on the solution  $\{\mathbf{u}_1, p_1\}$  to Eqs. (15)–(18). Due to its linearity, we can decompose this system of equations into two sub-problems to better understand its solution structure:

$$\{\mathbf{u}_1, p_1\} = \{\mathbf{u}_1^D, p_1^D\} + \{\mathbf{u}_1^{NL}, p_1^{NL}\}. \quad (34)$$

The sub-problem  $\{\mathbf{u}_1^D, p_1^D\}$  takes the homogenous part of Eq. (16) (the Stokes equation) with the inhomogeneous boundary condition from Eq. (18)

$$\nabla \cdot \mathbf{u}_1^D = 0, \quad \nabla p_1^D = \nabla^2 \mathbf{u}_1^D, \quad (35)$$

$$\mathbf{u}_1^D(r=1) = \mathbf{0}, \quad \mathbf{u}_1^D(r \rightarrow \infty) = -\mathbf{U}_1; \quad (36)$$

the other sub-problem  $\{\mathbf{u}_1^{NL}, p_1^{NL}\}$  takes the inhomogeneous term in Eq. (16) with homogenous boundary conditions

$$\nabla \cdot \mathbf{u}_1^{NL} = 0, \quad \nabla p_1^{NL} = \nabla^2 \mathbf{u}_1^{NL} + \nabla \cdot \mathbf{A}, \quad (37)$$



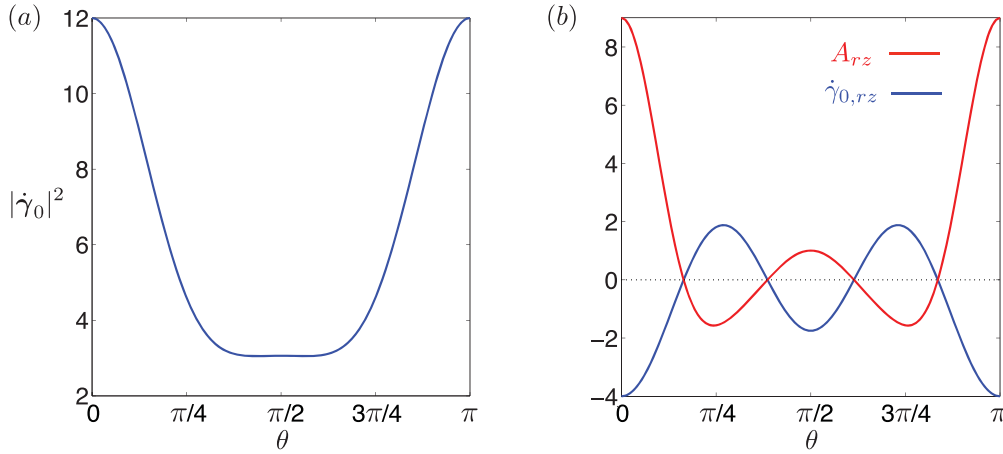


**Fig. 3.** (a) Magnitude of the rate-of-strain tensor  $|\dot{\gamma}_0|^2$  as a function of  $\theta$  on the squirmer surface ( $r = 1$ ) for a third-mode squirmer in Stokes flow. (b) The  $rz$ -components of the rate-of-strain tensor ( $\dot{\gamma}_{0,rz}$ ) based on the Stokes flow solution (blue line) and local shear stress reduction ( $A_{rz}$ ) due to shear-thinning viscosity (red line) as a function of  $\theta$  on the squirmer surface ( $r = 1$ ) with a third mode. (For interpretation of the references to color in this figure legend, the reader is referred to the web version of this article.)

$$\mathbf{u}_1^{\text{NL}}(r = 1) = \mathbf{0}, \quad \mathbf{u}_1^{\text{NL}}(r \rightarrow \infty) = \mathbf{0}. \quad (38)$$

It can be readily recognized that the solution  $\{\mathbf{u}_1^{\text{D}}, p_1^{\text{D}}\}$  to the sub-problem governed by Eqs. (35)–(36) represents the classical solution of a Stokes flow past a sphere. Under the decomposition in Eq. (34), we rewrite the non-Newtonian correction to stress around a squirmer  $\boldsymbol{\sigma}_1$  in Eq. (33) as

$$\boldsymbol{\sigma}_1 = \underbrace{-p_1^{\text{D}}\mathbf{I} + \dot{\gamma}_1^{\text{D}}}_{\text{Stokes drag}} + \underbrace{-p_1^{\text{NL}}\mathbf{I} + \dot{\gamma}_1^{\text{NL}}}_{\text{Non-local effect}} + \underbrace{\mathbf{A}}_{\text{Local effect}}, \quad (39)$$

which represent three different physical effects. The solutions  $\{\mathbf{u}_1^{\text{D}}, p_1^{\text{D}}\}$  to Eqs. (35) and  $\{\mathbf{u}_1^{\text{NL}}, p_1^{\text{NL}}\}$  to Eqs. (37) and (38), respectively, contribute the terms  $-p_1^{\text{D}}\mathbf{I} + \dot{\gamma}_1^{\text{D}}$  (referred to as “Stokes drag”) and  $-p_1^{\text{NL}}\mathbf{I} + \dot{\gamma}_1^{\text{NL}}$  (referred to as “non-local effect”) in Eq. (39). The last term  $\mathbf{A}$  in the equation (referred to as “local effect”) is given by Eq. (17), which depends only on the zeroth order flow (i.e., Stokes flow).

We first focus on the local effect represented by the tensor  $\mathbf{A} = (1 - \beta)(n - 1)|\dot{\gamma}_0|^2\dot{\gamma}_0/2$  in Eq. (39), which has a structure of a viscosity correction  $[(1 - \beta)(n - 1)|\dot{\gamma}_0|^2/2]$  multiplied by the rate-of-strain tensor  $\dot{\gamma}_0$ . This can be interpreted physically as a local correction to the shear stress due to viscosity reduction. Under this perturbative framework, both the viscosity reduction and the rate-of-strain tensor in  $\mathbf{A}$  are calculated based on the zeroth-order order flow (i.e., Stokes flow). That is, to leading order, this local effect accounts for viscosity reduction assuming that the flow field remains the same as the Newtonian case.

In this perturbative framework, the (non-local) effect of the flow induced by spatial variations of the viscosity throughout the fluid are accounted for by the second term on the right-hand side in Eq. (39). The decomposition in Eq. (34) isolates the non-local effect of induced changes in the flow, which are described by  $\{\mathbf{u}_1^{\text{NL}}, p_1^{\text{NL}}\}$  in the sub-problem governed by Eqs. (37) and (38). The shear-thinning effect manifests as a source of extra stress,  $\nabla \cdot \mathbf{A}$ , driving a fluid flow  $\mathbf{u}_1^{\text{NL}}$  and its associated pressure field  $p_1^{\text{NL}}$ , as shown in Fig. 2b & d respectively. We remark that, while the local effect represented by  $\mathbf{A}$  in Eq. (39) accounts for viscosity reduction but not flow changes, here the non-local effect represented by  $-p_1^{\text{NL}}\mathbf{I} + \dot{\gamma}_1^{\text{NL}}$ , complementarily, accounts for flow changes while assuming uniform fluid viscosity (note that Eq. (37) has the form of an inhomogeneous or “forced” Stokes equation with Newtonian rheology). Taken together, this weakly non-linear analysis decouples the two types of physical changes when the fluid becomes shear-thinning, namely viscosity reduction and flow changes, into two separate problems and addresses these effects individually in each problem.

Finally, the remaining term,  $-p_1^{\text{D}}\mathbf{I} + \dot{\gamma}_1^{\text{D}}$ , in Eq. (39) corresponds to the Stokes flow past a sphere due to a uniform flow  $-\mathbf{U}_1$  in the far

field. This uniform flow emerges, passively, as a result of the local effect through  $\mathbf{A}$  and the non-local effect through  $-p_1^{\text{NL}}\mathbf{I} + \dot{\gamma}_1^{\text{NL}}$  to satisfy the overall force-free condition,  $\int_S \boldsymbol{\sigma}_1 \cdot \mathbf{n} \, dS = \mathbf{0}$ . We integrate Eq. (39) over the squirmer surface to obtain the net force acting on the squirmer at this order

$$\begin{aligned} \int_S \boldsymbol{\sigma}_1 \cdot \mathbf{n} \, dS &= \int_S (-p_1^{\text{D}}\mathbf{I} + \dot{\gamma}_1^{\text{D}}) \cdot \mathbf{n} \, dS + \int_S (-p_1^{\text{NL}}\mathbf{I} + \dot{\gamma}_1^{\text{NL}}) \cdot \mathbf{n} \, dS \\ &\quad + \int_S \mathbf{A} \cdot \mathbf{n} \, dS. \end{aligned} \quad (40)$$

The net force above contains a local contribution due to the effect of local viscosity reduction ( $F_1^{\text{L}}$ ) and a non-local contribution due to the induced flow ( $F_1^{\text{NL}}$ ). These two forces compete and give rise to the motion of the squirmer  $\mathbf{U}_1$  and hence the Stokes drag  $F_1^{\text{D}} = -\mathbf{R} \cdot \mathbf{U}_1 = -6\pi\mathbf{U}_1$ . We reiterate that the Stokes drag emerges passively to counter balance the difference between the two driving forces  $F_1^{\text{L}}$  and  $F_1^{\text{NL}}$  so that the overall force-free condition is satisfied  $F_1^{\text{D}} + F_1^{\text{NL}} + F_1^{\text{L}} = \mathbf{0}$ . Inverting the resistance we then obtain the velocity

$$\mathbf{U}_1 = \frac{1}{6\pi} [F_1^{\text{NL}} + F_1^{\text{L}}] \quad (41)$$

as dictated by Eq. (6). In other words, the relative magnitudes and directions of  $F_1^{\text{L}}$  and  $F_1^{\text{NL}}$  dictate the dynamics of a squirmer in a shear-thinning fluid.

In the next sections, we illustrate the above decomposition and quantify the two driving forces using a specific example of a third-mode squirmer, which clearly elucidates how local and non-local effects generate self-propulsion otherwise absent in a Newtonian fluid; similar analyses can be applied to other squirmers as well.

#### 4.3.1. Effect of local viscosity reduction

The analysis of the effect of local viscosity reduction follows the same spirit of previous studies that looked into the viscosity distribution around a swimmer [30,31,33]. In this perturbative framework, to leading order, one assumes the flow field does not change and uses the Stokes flow around a squirmer (Eqs. (27) and (28); Fig. 2a) to deduce the contribution from local viscosity reduction. Based on the Stokes solution given in Eqs. (27) and (28), we quantify how much shearing is around the squirmer by calculating the magnitude of the rate-of-strain tensor on the squirmer surface (Fig. 3a). For a third-mode

**Table 1**

The decomposition of the first-order force acting on a squirmer into different components. All forces are along the  $z$ -direction due to axisymmetry; the numerical values below are the  $z$ -component of the corresponding force components. All values are multiplied by  $\pi(1-\beta)(1-n)$ .

Mode	$F_1^D$	$F_{1,\gamma}^{NL}$	$F_{1,p_1}^{NL}$	$F_1^{NL} = F_{1,\gamma_1}^{NL} + F_{1,p_1}^{NL}$	$F_1^L$
$B_1$	0.985	6.564	-16.082	-9.518	8.533
$B_1$ & $B_2$	$0.985 + 2.211\alpha^2$	$6.564 + 21.603\alpha^2$	$-16.082 - 24.164\alpha^2$	$-9.518 - 13.639\alpha^2$	$8.533 + 11.429\alpha^2$
$B_3$	0.121	1.850	-3.855	-2.005	1.884
$B_5$	0.020	0.478	-1.623	-1.144	1.124

squirmer, fluid shearing is most substantial in regions near the poles ( $\theta = 0, \pi$ ) compared with the equator ( $\theta = \pi/2$ ). Shear-thinning rheology, thus, will cause the most significant reduction in viscosity, and hence shear stress, near the poles. In Fig. 3b, we compare the viscous traction along the propulsion direction ( $z$ ) in Stokes flow,  $\dot{\gamma}_{0,rz}$  (blue line), with the modification due to the local shear-thinning effect along the same direction,  $A_{rz}$  (red line). In Stokes flow, we observe that the viscous tractions at the poles act to push the squirmer in the negative  $z$ -direction (downward). Since the shear-thinning effect is most substantial around the poles, the tractions acting downward (negative  $z$ -direction) in these regions are reduced by the shear-thinning effect more significantly than other regions on the squirmer surface, as shown by the variation of  $A_{rz}$  in Fig. 3b. We note that  $A_{rz}$  has its sign opposite to  $\dot{\gamma}_{0,rz}$  while its magnitude is modulated by variations of  $|\dot{\gamma}_{0,rz}|^2$ , a manifestation of the shear-thinning effect. In Stokes flows, the viscous traction around a third-mode squirmer integrates to zero ( $\int_S \dot{\gamma}_0 \cdot \mathbf{n} \, dS = \int_S \dot{\gamma}_{0,rz} \, dS \, \mathbf{e}_z = \mathbf{0}$ ). In contrast, locally varying magnitudes of shear-thinning perturbs this zero balance; relatively more significant reductions in the downward forces at the poles result in a net upward force ( $F_1^L = \int_S \mathbf{A} \cdot \mathbf{n} \, dS = \int_S A_{rz} \, dS \, \mathbf{e}_z$ ) on the squirmer. Hence, if one only focuses on the local effect of viscosity changes, assuming the flow field does not change, one may argue that the squirmer with a positive third mode will propel upward, in contradistinction to the result obtained in Eq. (32).

#### 4.3.2. Effect of induced changes in the flow

To capture the second physical change due to shear-thinning, namely the change in the flow field, one considers the complementary problem (Eqs. (37) and (38)) where the fluid is assumed to have uniform viscosity but with  $\nabla \cdot \mathbf{A}$  entering the Stokes equation as a source of extra stress. The structure of this extra term  $\nabla \cdot \mathbf{A} = \nabla \cdot [(1-\beta)(n-1)|\dot{\gamma}_0|^2 \dot{\gamma}_0/2]$  resembles the viscous shear stress in Stokes flows  $\dot{\gamma}_0$ , but with an opposite sign and magnitude magnified unevenly depending on the local shear rate (through the pre-factor  $(1-\beta)(n-1)|\dot{\gamma}_0|^2/2$ ). In Fig. 2, we contrast velocity and pressure fields in Stokes flow with those induced by this extra stress to highlight several features of the induced changes in the flow.

First, due to the opposite sign of this extra stress, the induced velocity field  $\mathbf{u}_1^{NL}$  has a reversed direction (Fig. 2b) compared with the Stokes flow (Fig. 2a). Second, since there are larger shear rates at the poles, larger extra stresses, and hence stronger flows, are induced at these locations. We note that the integral of viscous traction vanishes for a third-mode squirmer in a Stokes flow. In contrast, the non-local flow exerts a net upward force (in the positive  $z$ -direction) on the squirmer surface via viscous traction,  $F_{1,\gamma_1}^{NL} = \int_S \dot{\gamma}_1^{NL} \cdot \mathbf{n} \, dS$ , where  $\dot{\gamma}_1^{NL}$  is the rate-of-strain tensor calculated using the velocity field  $\mathbf{u}_1^{NL}$  obtained from Eqs. (37) and (38). Table 1 details the numerical values of the force.

In addition to viscous traction, the pressure field associated with the non-local flow also exerts a net force on the squirmer,  $F_{1,p_1}^{NL} = \int_S -p_1^{NL} \mathbf{n} \, dS$ . Similar to the velocity field, the non-local pressure field also has a reversed sign and magnified strength at the poles (Fig. 2d) compared with the pressure field in the Stokes flow (Fig. 2c). We note

that the pressure around the squirmer integrates to zero in Stokes flow. In contrast, the pressure becomes dominant around the poles due to the shear-thinning effect, which gives rise to a net downward force (in the negative  $z$ -direction) on the squirmer.

Table 1 shows that the non-local force contribution of the pressure has a magnitude greater than that of the viscous traction,  $|F_{1,p_1}^{NL}| > |F_{1,\gamma_1}^{NL}|$ . Combining these two forces due to the non-local flow,  $F_1^{NL} = F_{1,\gamma_1}^{NL} + F_{1,p_1}^{NL}$ , results in a net downward force on the squirmer. Furthermore, because the force due to the non-local effect is stronger than that due to the local effect,  $|F_1^{NL}| > |F_1^L|$ , the third-mode squirmer goes downward as shown by Eq. (32). The dominance of the non-local effect over the local effect is also observed for squirmers with other modes of surface velocity (see Table 1).

This detailed example illustrates the importance of the non-local shear-thinning effect due to induced changes in the flow. If one focuses only on the stress reduction due to local viscosity changes without considering changes to the flow field, a qualitatively incorrect conclusion about the propulsion direction may result.

## 5. Conclusion

Results in this work complement our previous study of a squirmer in a shear-thinning fluid via the reciprocal theorem [39] by examining the surrounding flow. We derived, for small  $Cu$ , an asymptotic, analytical solution describing the velocity and pressure fields around squirmers with different modes of surface velocity. There are two types of physical changes that impact locomotion when the fluid shear thins [34,38]: the first change (local) is the reduction in shear stress due to local viscosity reduction, and the second change (non-local) is the stress induced by a modification of the overall fluid flow. Our asymptotic analysis examines these two effects individually via the decomposition in Eq. (39). This enabled a more systematic understanding of individual effects and a quantitative comparison of their relative contributions to locomotion in a shear-thinning fluid. A recent empirical model, focusing on only the local viscosity reduction effect, was shown to qualitatively capture the main physical features of swimming in a shear-thinning fluid for slender bodies [34]. Here, via a spherical squirmer model, we reveal cases where the local effect due to viscosity reduction is subdominant to the non-local effect due to induced changes in the flow. These results suggest that the relative magnitudes of the local and non-local effects may depend significantly on the details of the geometry and gait of the swimmer. One should thus exercise caution when predicting dynamics from the local viscosity distribution around a swimmer in a shear-thinning fluid.

## Acknowledgments

Funding by the National Science Foundation (Grant no. EFMA-1830958 to O.S.P), the Natural Sciences and Engineering Research Council of Canada (Grant no. RGPIN-2014-06577 to G.J.E.), and the Swedish Research Council (through a VR International Postdoc Grant 2015-06334 to L.Z) is gratefully acknowledged.

**Appendix A. Detailed solution procedures for determining the flow around a squirmer**

In this appendix, we illustrate the solution process for a neutral squirmer ( $\alpha = 0$ ); the same procedures apply to other squirming modes as well. Using the zeroth-order velocity field in Eqs. (12) and (13) for a neutral squirmer, Eq. (21) becomes

$$E^2(E^2\psi) = -\frac{8 \sin^2 \theta}{r^{13}}(53 + 15 \cos 2\theta)(1 - \beta)(n - 1). \tag{A.1}$$

We substitute the assumed form of solution given by Eq. (23) into Eq. (A.1) to obtain a system of ordinary differential equations by orthogonality

$$f_0'''' - \frac{4}{r^2}f_0'' + \frac{8}{r^3}f_0' - \frac{8}{r^4}f_0 - \frac{12}{r^2}f_2'' + \frac{24}{r^3}f_2' + \frac{48}{r^4}f_2 = -\frac{424}{r^{13}}, \tag{A.2}$$

$$f_1'''' - \frac{12}{r^2}f_1'' + \frac{24}{r^3}f_1' = 0, \tag{A.3}$$

$$f_2'''' - \frac{24}{r^2}f_2'' + \frac{48}{r^3}f_2' + \frac{72}{r^4}f_2 = -\frac{120}{r^{13}}. \tag{A.4}$$

We note that the above equations are Cauchy–Euler equations, which we can solve to obtain

$$f_0 = \frac{A_0}{r} + B_0r + C_0r^2 + D_0r^4 + E_0r^6 + \frac{F_0}{r^3} + \frac{G_0}{r^9}, \tag{A.5}$$

$$f_1 = \frac{A_1}{r^2} + B_1r^3 + C_1r^5 + D_1, \tag{A.6}$$

$$f_2 = \frac{A_2}{r^3} + \frac{B_2}{r} + C_2r^4 + D_2r^6 + \frac{E_2}{r^9}, \tag{A.7}$$

where the coefficients are determined by applying the boundary conditions in Eq. (18).

The far field boundary condition  $u(r \rightarrow \infty) = -U_1$  dictates that

$$B_1 = C_1 = C_2 = D_0 = D_2 = E_0 = 0, \tag{A.8}$$

$$C_0 = -\frac{U_1}{2(1 - \beta)(n - 1)}, E_2 = -\frac{1}{78}, G_0 = -\frac{1}{26}, F_0 = \frac{3}{5}A_2. \tag{A.9}$$

The remaining coefficients are determined by the boundary condition  $u_1(r = 1) = \mathbf{0}$  on the squirmer surface to be

$$A_1 = D_1 = 0, A_2 = -\frac{2}{39}, B_2 = -\frac{1}{26}, F_0 = -\frac{2}{65}, \tag{A.10}$$

$$A_0 = -\frac{U_1}{4(1 - \beta)(n - 1)} + \frac{17}{130}, B_0 = \frac{3U_1}{4(1 - \beta)(n - 1)} - \frac{8}{65}. \tag{A.11}$$

These coefficients are expressed in terms of the first order swimming speed,  $U_1$ , which is determined by enforcing the force-free condition ( $\int_S \sigma_1 \cdot n dS = \mathbf{0}$ ) as

$$U_1 = (1 - \beta)(n - 1)\frac{32}{195} \tag{A.12}$$

for a neutral squirmer. The same procedures apply when considering squirmers with other modes of actuation.

**Appendix B. Streamfunction and pressure field around a two-mode squirmer**

The streamfunction for the flow around a squirmer with the  $B_1$  and  $B_2$  modes ( $\alpha = B_2/B_1$ ) is given by

$$\begin{aligned} \psi_1 = & (1 - \beta)(n - 1) \sin^2 \theta \left\{ -\left(\frac{c_1^{B_1}}{r^9} + \frac{c_2^{B_1}}{r^3} + \frac{c_3^{B_1}}{r} + c_4^{B_1} r\right) \right. \\ & - \cos 2\theta \left(\frac{c_5^{B_1}}{r^9} + \frac{c_6^{B_1}}{r^3} + \frac{c_7^{B_1}}{r}\right) \\ & + \left(\frac{c_1^\alpha}{r^{11}} + \frac{c_2^\alpha}{r^9} + \frac{c_3^\alpha}{r^7} + \frac{c_4^\alpha}{r^5} + \frac{c_5^\alpha}{r^3} + \frac{c_6^\alpha}{r} + c_7^\alpha r\right) \alpha^2 \\ & + \cos \theta \left[ \left(\frac{c_8^\alpha}{r^8} + \frac{c_9^\alpha}{r^{10}} + \frac{c_{10}^\alpha}{r^8} + \frac{c_{11}^\alpha}{r^4} + \frac{c_{12}^\alpha}{r^2}\right) \alpha + \left(c_{13}^\alpha + \frac{c_{14}^\alpha}{r^{12}} + \frac{c_{15}^\alpha}{r^{10}} + \frac{c_{16}^\alpha}{r^8} \right. \right. \\ & \left. \left. + \frac{c_{17}^\alpha}{r^6} + \frac{c_{18}^\alpha}{r^4} + \frac{c_{19}^\alpha}{r^2} + \frac{c_{20}^\alpha \log r}{r^6}\right) \alpha^3 \right] \\ & + \cos 2\theta \left(\frac{c_{21}^\alpha}{r^{11}} + \frac{c_{22}^\alpha}{r^9} + \frac{c_{23}^\alpha}{r^7} + \frac{c_{24}^\alpha}{r^5} + \frac{c_{25}^\alpha}{r^3} + \frac{c_{26}^\alpha}{r}\right) \alpha^2 \\ & + \cos 3\theta \left[ \left(\frac{c_{27}^\alpha}{r^{10}} + \frac{c_{28}^\alpha}{r^4} + \frac{c_{29}^\alpha}{r^2}\right) \alpha + \left(\frac{c_{30}^\alpha}{r^{12}} + \frac{c_{31}^\alpha}{r^{10}} + \frac{c_{32}^\alpha}{r^8} + \frac{c_{33}^\alpha}{r^6} + \frac{c_{34}^\alpha}{r^4} \right. \right. \\ & \left. \left. + \frac{c_{35}^\alpha}{r^2} + \frac{c_{36}^\alpha \log(r)}{r^6}\right) \alpha^3 \right] \\ & + \cos 4\theta \left(\frac{c_{37}^\alpha}{r^{11}} + \frac{c_{38}^\alpha}{r^7} + \frac{c_{39}^\alpha}{r^5} + \frac{c_{40}^\alpha}{r^3}\right) \alpha^2 \\ & + \cos 5\theta \left(\frac{c_{41}^\alpha}{r^{12}} + \frac{c_{42}^\alpha}{r^{10}} + \frac{c_{43}^\alpha}{r^8} + \frac{c_{44}^\alpha}{r^6} + \frac{c_{45}^\alpha}{r^4} + \frac{c_{46}^\alpha \log(r)}{r^6}\right) \alpha^3 \left. \right\} \\ & - \frac{\sin^2 \theta}{4} \left(\frac{1}{r} - 3r + 2r^2\right) U_1. \tag{B.1} \end{aligned}$$

The corresponding pressure field is given by

$$\begin{aligned} p_1 = & \frac{(1 - \beta)(n - 1)}{2} \left\{ \left[ \frac{e_1^{B_1}}{r^{12}} + \frac{e_2^{B_1}}{r^4} + \frac{e_3^{B_1}}{r^2} + \cos 2\theta \left(\frac{e_4^{B_1}}{r^{12}} + \frac{e_5^{B_1}}{r^4}\right) \right] \cos \theta \right. \\ & + \left(\frac{e_1^\alpha}{r^{13}} + \frac{e_2^\alpha}{r^{11}} + \frac{e_3^\alpha}{r^5} + \frac{e_4^\alpha}{r^3}\right) \alpha + \left(\frac{e_5^\alpha}{r^{15}} + \frac{e_6^\alpha}{r^{13}} + \frac{e_7^\alpha}{r^{11}} + \frac{e_8^\alpha}{r^9} + \frac{e_9^\alpha}{r^7} \right. \\ & \left. + \frac{e_{10}^\alpha}{r^5} + \frac{e_{11}^\alpha}{r^3}\right) \alpha^3 \\ & + \cos \theta \left(\frac{e_{12}^\alpha}{r^{14}} + \frac{e_{13}^\alpha}{r^{12}} + \frac{e_{14}^\alpha}{r^{10}} + \frac{e_{15}^\alpha}{r^6} + \frac{e_{16}^\alpha}{r^4} + \frac{e_{17}^\alpha}{r^2}\right) \alpha^2 \\ & + \cos 2\theta \left[ \left(\frac{e_{18}^\alpha}{r^{13}} + \frac{e_{19}^\alpha}{r^{11}} + \frac{e_{20}^\alpha}{r^5} + \frac{e_{21}^\alpha}{r^3}\right) \alpha + \left(\frac{e_{22}^\alpha}{r^{15}} + \frac{e_{23}^\alpha}{r^{13}} + \frac{e_{24}^\alpha}{r^{11}} + \frac{e_{25}^\alpha}{r^9} \right. \right. \\ & \left. \left. + \frac{e_{26}^\alpha}{r^7} + \frac{e_{27}^\alpha}{r^5} + \frac{e_{28}^\alpha}{r^3}\right) \alpha^3 \right] + \cos 3\theta \left(\frac{e_{29}^\alpha}{r^{14}} + \frac{e_{30}^\alpha}{r^{12}} + \frac{e_{31}^\alpha}{r^{10}} + \frac{e_{32}^\alpha}{r^6} + \frac{e_{33}^\alpha}{r^4}\right) \alpha^2 \\ & + \cos 4\theta \left[ \left(\frac{e_{34}^\alpha}{r^{13}} + \frac{e_{35}^\alpha}{r^{11}} + \frac{e_{36}^\alpha}{r^5}\right) \alpha + \left(\frac{e_{37}^\alpha}{r^{15}} + \frac{e_{38}^\alpha}{r^{13}} + \frac{e_{39}^\alpha}{r^{11}} + \frac{e_{40}^\alpha}{r^9} \right. \right. \\ & \left. \left. + \frac{e_{41}^\alpha}{r^7} + \frac{e_{42}^\alpha}{r^5}\right) \alpha^3 \right] \\ & + \cos 5\theta \left(\frac{e_{43}^\alpha}{r^{14}} + \frac{e_{44}^\alpha}{r^{12}} + \frac{e_{45}^\alpha}{r^{10}} + \frac{e_{46}^\alpha}{r^6}\right) \alpha^2 + \cos 6\theta \left(\frac{e_{47}^\alpha}{r^{15}} + \frac{e_{48}^\alpha}{r^{13}} + \frac{e_{49}^\alpha}{r^{11}} \right. \\ & \left. + \frac{e_{50}^\alpha}{r^9} + \frac{e_{51}^\alpha}{r^7}\right) \alpha^3 \left. \right\} + \frac{3}{2r^2} U_1 \cos \theta. \tag{B.2} \end{aligned}$$

The coefficients  $c_i^\alpha$  and  $e_i^\alpha$  are given in Tables C.1 and C.2.



**Appendix C. Coefficients in the streamfunctions and pressure fields**

**Table C.1**  
Coefficients associated with the streamfunction and pressure field around a squirmer with a  $B_1$  mode.

$i$	$c_i^{B_1}$	$e_i^{B_1}$
1	$\frac{1}{26}$	$-\frac{854}{39}$
2	$-\frac{2}{65}$	$\frac{2}{13}$
3	$-\frac{17}{130}$	$-\frac{32}{65}$
4	$\frac{8}{65}$	$-\frac{26}{3}$
5	$\frac{1}{78}$	$-\frac{10}{13}$
6	$-\frac{2}{39}$	
7	$\frac{1}{26}$	

**Table C.2**  
Coefficients associated with the streamfunction and pressure field around a squirmer with  $B_1$  and  $B_2$  modes.

$i$	$c_i^{\alpha}$	$e_i^{\alpha}$	$i$	$c_i^{\alpha}$	$e_i^{\alpha}$	$i$	$c_i^{\alpha}$	$e_i^{\alpha}$
1	$-\frac{40583}{134368}$	$-\frac{3751}{52}$	21	$-\frac{713}{2584}$	$-\frac{3858}{1001}$	41	$-\frac{45}{2432}$	$-\frac{1359}{7904}$
2	$\frac{24}{143}$	$\frac{431}{13}$	22	$\frac{1}{13}$	$-\frac{2631645}{20672}$	42	$\frac{15}{2432}$	$-\frac{7790587}{8129264}$
3	$\frac{161}{1716}$	$-\frac{9}{20}$	23	$\frac{21}{104}$	$\frac{235493}{1292}$	43	$\frac{3}{32}$	$-\frac{5865}{304}$
4	$\frac{3755}{235144}$	$-\frac{1286}{1001}$	24	$\frac{751}{25194}$	$-\frac{18093}{208}$	44	$-\frac{2121}{31616}$	$\frac{45}{2}$
5	$\frac{90109}{361760}$	$-\frac{2148967}{31008}$	25	$\frac{10243}{25194}$	$\frac{2016}{143}$	45	$-\frac{453}{31616}$	$-\frac{27}{4}$
6	$\frac{52729}{1021020}$	$\frac{3323573}{33592}$	26	$-\frac{1165}{2652}$	$-\frac{2265}{15808}$	46	$\frac{27}{208}$	$-\frac{72603}{67184}$
7	$-\frac{1383}{5005}$	$-\frac{6687}{143}$	27	$-\frac{1}{24}$	$-\frac{1112941}{2032316}$	47		$-\frac{465}{64}$
8	$-\frac{643}{1001}$	$\frac{16967}{2288}$	28	$\frac{1}{6}$	$-\frac{32667}{17017}$	48		$\frac{1005}{76}$
9	$-\frac{25}{104}$	$-\frac{3775}{55328}$	29	$-\frac{1}{8}$	$-\frac{539765}{5168}$	49		$-\frac{135}{16}$
10	$\frac{5}{143}$	$-\frac{10016469}{40646320}$	30	$-\frac{3865}{41344}$	$\frac{213}{2}$	50		$\frac{9}{4}$
11	$\frac{3}{14}$	$-\frac{10889}{17017}$	31	$\frac{2683}{41344}$	$-\frac{1413}{52}$	51		$-\frac{4983}{15808}$
12	$\frac{5073}{8008}$	$-\frac{617929}{2584}$	32	$\frac{3}{16}$	$-\frac{40335}{67184}$			
13	$-\frac{10889}{34034}$	$\frac{2915}{13}$	33	$-\frac{672129}{3825536}$	$-\frac{5825}{1326}$			
14	$-\frac{7605}{20672}$	$-\frac{7497}{143}$	34	$\frac{5543347}{65034112}$	$-\frac{65}{4}$			
15	$\frac{103239}{268736}$	$-\frac{121005}{235144}$	35	$-\frac{1112941}{16258528}$	<b>9</b>			
16	$\frac{681}{4576}$	$-\frac{1165}{442}$	36	$\frac{405}{2288}$	$-\frac{7}{4}$			
17	$-\frac{457423}{1912768}$	$-\frac{5532}{5005}$	37	$-\frac{505}{10336}$	$-\frac{20795}{608}$			
18	$\frac{1978583}{17509184}$	$-\frac{95}{604}$	38	$\frac{9}{104}$	$\frac{138675}{2584}$			
19	$\frac{2459935}{8754592}$	$\frac{604}{13}$	39	$\frac{751}{33592}$	$-\frac{57}{2}$			
20	$\frac{225}{1144}$	$-1$	40	$-\frac{8067}{134368}$	$\frac{1143}{208}$			

**Table C.3**  
Coefficients associated with the streamfunction and pressure field around a squirmer with a  $B_3$  mode.

$i$	$c_i^{B_3}$	$e_i^{B_3}$	$i$	$c_i^{B_3}$	$e_i^{B_3}$
1	$\frac{3922425}{14319616}$	$-\frac{227754473}{3579904}$	21	$-\frac{370605}{1789952}$	$\frac{12420825}{661504}$
2	$-\frac{111082089}{243433472}$	$\frac{3438978135}{30429184}$	22	$-\frac{265545}{5292032}$	$-\frac{45405}{94208}$
3	$\frac{42001851}{275185664}$	$-\frac{352609945}{5292032}$	23	$\frac{217862315}{1551888384}$	$\frac{102707919}{258648064}$
4	$\frac{2566907559103}{4231275408888}$	$\frac{1373496101}{103194624}$	24	$-\frac{1092141855}{26899398656}$	$-\frac{21350955}{12361836}$
5	$-\frac{2628194625}{107597594624}$	$-\frac{241963245}{1023852544}$	25	$-\frac{483342523}{1349699328}$	$-\frac{16429}{512}$
6	$-\frac{29550956425}{1035626848256}$	$\frac{604835523}{2845128704}$	26	$\frac{7116985}{148342272}$	$\frac{5508825}{94208}$
7	$-\frac{17975181871}{247484357120}$	$-\frac{206392565}{259598976}$	27	$-\frac{39375}{330752}$	$-\frac{73125}{2048}$
8	$\frac{2353040961}{29590520960}$	$\frac{3360863}{5240352}$	28	$\frac{17577}{376832}$	$\frac{286875}{38912}$
9	$\frac{269768}{17782765}$	$-\frac{1079072}{17782765}$	29	$-\frac{20955}{376832}$	$\frac{227025}{894976}$
10	$-\frac{12403125}{189190144}$	$-\frac{3105401}{11776}$	30	$-\frac{5775}{77824}$	$-\frac{445067649}{517296128}$
11	$\frac{3193605}{7159808}$	$\frac{806206965}{1789952}$	31	$\frac{48721965}{517296128}$	$-\frac{74375}{8192}$
12	$-\frac{89849055}{121716736}$	$-\frac{168637785}{661504}$	32	$-\frac{2479545}{89964544}$	$\frac{75075}{4096}$
13	$\frac{292515}{1323008}$	$\frac{94512191}{1984512}$	33	$\frac{34235973}{2069184512}$	$-\frac{212625}{16384}$
14	$\frac{32584874177}{262269136896}$	$\frac{3223755}{11634688}$	34	$-\frac{16875}{165376}$	$\frac{31875}{8192}$
15	$-\frac{13881408975}{295893385216}$	$-\frac{4416440517}{5690257408}$	35	$\frac{315}{32768}$	$-\frac{3859425}{7159808}$
16	$-\frac{46539750865}{887680155648}$	$\frac{7116985}{9271392}$	36	$-\frac{6405}{753664}$	
17	$-\frac{302811661}{2651618112}$	$-\frac{16804315}{5240352}$	37	$-\frac{2625}{65536}$	
18	$\frac{3360863}{20961408}$	$-\frac{4166659}{47104}$	38	$\frac{222045}{7159808}$	
19	$-\frac{275625}{2149888}$	$\frac{7336695}{47104}$	39	$\frac{227025}{28639232}$	
20	$\frac{6849}{47104}$	$-\frac{7144765}{77824}$	40	$-\frac{5625}{77824}$	

**References**

- [1] E.M. Purcell, Life at low Reynolds number, *Am. J. Phys.* 45 (1977) 3–11.
- [2] C. Brennen, H. Winet, Fluid mechanics of propulsion by cilia and flagella, *Annu. Rev. Fluid Mech.* 9 (1977) 339–398.
- [3] D. Bray, *Cell Movements*, Garland Publishing, New York, NY, 2000.
- [4] L.J. Fauci, R. Dillon, *Biofluidmechanics of reproduction*, *Annu. Rev. Fluid Mech.* 38 (2006) 371–394.
- [5] E. Lauga, T.R. Powers, The hydrodynamics of swimming microorganisms, *Rep. Prog. Phys.* 72 (2009) 096601.
- [6] E. Lauga, *Bacterial hydrodynamics*, *Annu. Rev. Fluid Mech.* 48 (2016) 105–130.
- [7] R. Dreyfus, J. Baudry, M.L. Roper, M. Fermigier, H.A. Stone, J. Bibette, Microscopic artificial swimmers, *Nature* 437 (7060) (2005) 862–865.
- [8] W.F. Paxton, S. Sundararajan, T.E. Mallouk, A. Sen, Chemical locomotion, *Angew. Chem. Int. Ed.* 45 (33) (2006) 5420–5429.
- [9] L. Zhang, J.J. Abbott, L. Dong, K.E. Peyer, B.E. Kratochvil, H. Zhang, C. Bergeles, B.J. Nelson, Characterizing the swimming properties of artificial bacterial flagella, *Nano Lett.* 9 (10) (2009) 3663–3667.
- [10] A. Ghosh, P. Fischer, Controlled propulsion of artificial magnetic nanostructured propellers, *Nano Lett.* 9 (6) (2009) 2243–2245.
- [11] S.J. Ebbens, J.R. Howse, In pursuit of propulsion at the nanoscale, *Soft Matter* 6 (2010) 726–738.
- [12] J.L. Moran, J.D. Posner, Phoretic self-propulsion, *Annu. Rev. Fluid Mech.* 49 (2017) 511–540.
- [13] J. Elgeti, R.G. Winkler, G. Gompper, Physics of microswimmers –single particle motion and collective behavior: a review, *Rep. Prog. Phys.* 78 (5) (2015) 056601.
- [14] E.W. Merrill, Rheology of blood, *Physiol. Rev.* 49 (1969) 863–888.
- [15] S.K. Lai, Y.Y. Wang, D. Wirtz, J. Hanes, Micro- and macrorheology of mucus, *Adv. Drug Deliv. Rev.* 61 (2009) 86–100.
- [16] M. Brust, C. Schaefer, R. Doerr, L. Pan, M. Garcia, P.E. Arratia, C. Wagner, Rheology of human blood plasma: viscoelastic versus Newtonian behavior, *Phys. Rev. Lett.* 110 (2013) 078305.
- [17] A.E. Pattenon, A. Gopinath, P.E. Arratia, Active colloids in complex fluids, *Curr. Opin. Colloid Interface Sci.* 21 (2016) 86–96.
- [18] E. Lauga, The bearable goeyness of swimming, *J. Fluid Mech.* 762 (2015) 1–4.
- [19] E. Lauga, Propulsion in a viscoelastic fluid, *Phys. Fluids* 19 (8) (2007) 083104.
- [20] H.C. Fu, C.W. Wolgemuth, T.R. Powers, Swimming speeds of filaments in nonlinearly viscoelastic fluids, *Phys. Fluids* 21 (2009) 033102.
- [21] J. Teran, L. Fauci, M. Shelley, Viscoelastic fluid response can increase the speed and efficiency of a free swimmer, *Phys. Rev. Lett.* 104 (2010) 038101.
- [22] Y. Bozorgi, P.T. Underhill, Effects of elasticity on the nonlinear collective dynamics of self-propelled particles, *J. Non-Newton. Fluid Mech.* 214 (2014) 69–77.
- [23] J. Sznitman, P.E. Arratia, Locomotion through complex fluids: an experimental view, in: S.E. Spagnolie (Ed.), *Complex Fluids in Biological Systems*, Springer, New York, 2015, pp. 245–281.

- [24] G.J. Elfring, E. Lauga, Theory of locomotion through complex fluids, in: S.E. Spagnolie (Ed.), *Complex Fluids in Biological Systems*, Springer, New York, 2015, pp. 283–317.
- [25] G.J. Elfring, G. Goyal, The effect of gait on swimming in viscoelastic fluids, *J. Non-Newton. Fluid Mech.* 234 (2016) 8–14.
- [26] G. Li, A.M. Ardekani, Collective motion of microorganisms in a viscoelastic fluid, *Phys. Rev. Lett.* 117 (2016) 118001.
- [27] B. Thomases, R.D. Guy, The role of body flexibility in stroke enhancements for finite-length undulatory swimmers in viscoelastic fluids, *J. Fluid Mech.* 825 (2017) 109?132.
- [28] R.B. Bird, R.C. Armstrong, O. Hassager, *Dynamics of Polymeric Liquids. Vol. 1: Fluid Mechanics*, John Wiley and Sons Inc., New York, 1987.
- [29] M. Dasgupta, B. Liu, H.C. Fu, M. Berhanu, K.S. Breuer, T.R. Powers, A. Kudrolli, Speed of a swimming sheet in Newtonian and viscoelastic fluids, *Phys. Rev. E* 87 (2013) 013015.
- [30] T.D. Montenegro-Johnson, A.A. Smith, D.J. Smith, D. Loghin, J.R. Blake, Modelling the fluid mechanics of cilia and flagella in reproduction and development, *Eur. Phys. J. E* 35 (2012) 1–17.
- [31] T.D. Montenegro-Johnson, D.J. Smith, D. Loghin, Physics of rheologically enhanced propulsion: different strokes in generalized stokes, *Phys. Fluids* 25 (2013) 081903.
- [32] J.R. Véllez-Cordero, E. Lauga, Waving transport and propulsion in a generalized Newtonian fluid, *J. Non-Newton Fluid* 199 (2013) 37–50.
- [33] G. Li, A.M. Ardekani, Undulatory swimming in non-Newtonian fluids, *J. Fluid Mech.* 784 (2015) R4.
- [34] E.E. Riley, E. Lauga, Empirical resistive-force theory for slender biological filaments in shear-thinning fluids, *Phys. Rev. E* 95 (2017) 062416.
- [35] J. Park, D. Kim, J.H. Shin, D.A. Weitz, Efficient nematode swimming in a shear thinning colloidal suspension, *Soft Matter* 12 (2016) 1892–1897.
- [36] D.A. Gagnon, N.C. Keim, P.E. Arratia, Undulatory swimming in shear-thinning fluids: experiments with *Caenorhabditis elegans*, *J. Fluid Mech.* 758 (2014) R3.
- [37] D.A. Gagnon, P.E. Arratia, The cost of swimming in generalized Newtonian fluids: experiments with *C. elegans*, *J. Fluid Mech.* 800 (2016) 753–765.
- [38] S. Gómez, F.A. Godínez, E. Lauga, R. Zenit, Helical propulsion in shear-thinning fluids, *J. Fluid Mech.* 812 (2017) R3.
- [39] C. Datt, L. Zhu, G.J. Elfring, O.S. Pak, Squirming through shear-thinning fluids, *J. Fluid Mech.* 784 (2015) R1.
- [40] C. Datt, G. Natale, S.G. Hatzikiriakos, G.J. Elfring, An active particle in a complex fluid, *J. Fluid Mech.* 823 (2017) 675–688.
- [41] H. Nganguia, K. Pietrzyk, O.S. Pak, Swimming efficiency in a shear-thinning fluid, *Phys. Rev. E* 96 (2017) 062606.
- [42] T. Qiu, T.C. Lee, A.G. Mark, K.I. Morozov, R. Münster, O. Mierka, S. Turek, A.M. Le-shansky, P. Fischer, Swimming by reciprocal motion at low Reynolds number, *Nat. Commun.* 5 (2014) 5119.
- [43] T.D. Montenegro-Johnson, Fake  $\mu$ s: a cautionary tail of shear-thinning locomotion, *Phys. Rev. Fluids* 2 (2017) 081101.
- [44] G. Li, A.M. Ardekani, Near wall motion of undulatory swimmers in non-Newtonian fluids, *Eur. J. Comput. Mech.* 26 (2017) 44–60.
- [45] Z. Ouyang, J. Lin, X. Ku, The hydrodynamic behavior of a squirmer swimming in power-law fluid, *Phys. Fluids* 30 (8) (2018) 083301.
- [46] J. Happel, H. Brenner, *Low Reynolds Number Hydrodynamics: With Special Applications to Particulate Media*, Noordhoff International Publishing, 1973.
- [47] H.A. Stone, A.D.T. Samuel, Propulsion of microorganisms by surface distortions, *Phys. Rev. Lett.* 77 (1996) 4102–4104.
- [48] E. Lauga, Locomotion in complex fluids: integral theorems, *Phys. Fluids* 26 (2014) 081902.
- [49] G.J. Elfring, A note on the reciprocal theorem for the swimming of simple bodies, *Phys. Fluids* 27 (2) (2015) 023101.
- [50] M.J. Lighthill, On the squirming motion of nearly spherical deformable bodies through liquids at very small Reynolds numbers, *Commun. Pure Appl. Math.* 5 (1952) 109–118.
- [51] J.R. Blake, A spherical envelope approach to ciliary propulsion, *J. Fluid Mech.* 46 (1971) 199–208.
- [52] T.J. Pedley, Spherical squirmers: models for swimming micro-organisms, *IMA J. Appl. Math.* 81 (2016) 488–521.
- [53] K. Drescher, K.C. Leptos, I. Tuval, T. Ishikawa, T.J. Pedley, R.E. Goldstein, Dancing volvox: hydrodynamic bound states of swimming algae, *Phys. Rev. Lett.* 102 (2009) 168101.
- [54] V. Magar, T. Goto, T.J. Pedley, Nutrient uptake by a self-propelled steady squirmer, *Q. J. Mech. Appl. Math.* 56 (2003) 65–91.
- [55] T. Ishikawa, T.J. Pedley, Coherent structures in monolayers of swimming particles, *Phys. Rev. Lett.* 100 (2008) 088103.
- [56] S. Wang, A. Ardekani, Inertial squirmer, *Phys. Fluids* 24 (2012) 101902.
- [57] L. Zhu, E. Lauga, L. Brandt, Self-propulsion in viscoelastic fluids: pushers vs. pullers, *Phys. Fluids* 24 (5) (2012) 051902.
- [58] S. Michelin, E. Lauga, D. Bartolo, Spontaneous autophoretic motion of isotropic particles, *Phys. Fluids* 25 (2013) 061701.
- [59] S. Yazdi, A.M. Ardekani, A. Borhan, Swimming dynamics near a wall in a weakly elastic fluid, *J. Nonlinear Sci.* 25 (2015) 1153–1167.
- [60] N.G. Chisholm, D. Legendre, E. Lauga, A.S. Khair, A squirmer across Reynolds numbers, *J. Fluid Mech.* 796 (2016) 233–256.
- [61] S.H. Hwang, M. Litt, W.C. Forsman, Rheological properties of mucus, *Rheol. Acta* 8 (1969) 438–448.
- [62] G.J. Elfring, Force moments of an active particle in a complex fluid, *J. Fluid. Mech.* 829 (2017) R3.